Available online at www.sciencedirect.com
ScienceDirect
Journal of Magnetic Resonance 183 (2006) 50–59
JMR Journal of Magnetic Resonance
www.elsevier.com/locate/jmr

# Area-selective signal parameter estimation for two-dimensional MR spectroscopy data ☆

Niclas Sandgren [a,*], Petre Stoica [a], Frederick J. Frigo [b]

[a] Systems and Control Division, Department of Information Technology, Uppsala University, P.O. Box 337, SE-751 05 Uppsala, Sweden
[b] GE Healthcare Technologies, Magnetic Resonance Business Group, P.O. Box 414 WTE-893, Milwaukee, WI 53201, USA

Received 20 March 2006; revised 24 June 2006
Available online 10 August 2006

**Abstract**

We consider the problem of parametric spectral analysis of two-dimensional (2D) magnetic resonance spectroscopy (MRS) data. Estimating the signal components from 2D MRS data is becoming common practice in many clinical MR applications. The most frequently used signal processing tool for this estimation problem is the non-parametric 2D-FFT. There are several alternative parametric methods available to perform this analysis, yet their computational complexity is generally rather high and it becomes prohibitive when the number of points in the measured data matrix is large. In this paper, we propose a novel signal parameter estimation technique which operates on a pre-specified sub-area of the 2D spectrum. This area-selective approach can be used either to estimate only the signal components of main interest in the data, or to compute signal parameter estimates of all present signal components as the computational burden for each sub-area is low. In the numerical example section we consider both simulated data and in vitro $^{1}$H data acquired from a 1.5 T MR scanner.


*Keywords:* Two-dimensional (2D) magnetic resonance spectroscopy; Damped sinusoidal model; Parametric area-selective analysis

## 1. Introduction

The use of two-dimensional (2D) spectral analysis techniques for quantitation of 2D MRS data has been emphasized in numerous papers published in the last decades. One of the first references introducing the 2D-FT (Fourier Transform) to the MR community was [1]. As a non-parametric spectral analysis method the 2D-FFT (Fast FT) is still widely used even though it suffers from several limitations such as poor resolution and high-sidelobe effects (see [2] and the references therein). The inability to distinguish between signal and noise is another general drawback of a non-parametric approach. As a consequence a significant number of parametric spectral analysis techniques, which can be applied to 2D MRS data, have been developed in recent years. The previous literature on 2D parametric spectral analysis includes the linear prediction (LP) approach (see, e.g., [3,4]), the matrix enhancement and matrix pencil (MEMP) method (see [5–7]), the 2D-ESPRIT method (see [8,9]), and the 2D-DMUSIC of [10]. The 2D frequency estimation problem is also closely related to the joint azimuth/elevation estimation in array signal processing (see, e.g., [11–14]).

One of the main problems of the parametric approach is its relatively high computational burden. Already in the one-dimensional (1D) case the computational complexity of a parametric technique involving, for example, an SVD (singular value decomposition) of a data matrix can be significant since the measured FID (free induction decay) typically contains thousands of samples. The attempt to reduce this significant computational complexity is one of the main reasons why several papers have been published recently on frequency-selective spectral analysis for 1D MRS data (see, e.g., [15–21]). In a 2D scenario this

☆ This work was partly supported by the Swedish Science Council (VR).
* Corresponding author. Fax: +46 18 51 19 25.
*E-mail address:* niclas.sandgren@it.uu.se (N. Sandgren).

1090-7807/$ - see front matter © 2006 Elsevier Inc. All rights reserved.
doi:10.1016/j.jmr.2006.07.018

computational-complexity problem increases dramatically with increasing the number of points and frames in the collected data matrix. In this paper, we consider a frequency-selective approach for 2D MRS data, which we refer to as area-selective spectral analysis. The only previously presented method (to the authors knowledge) which considers area-selective spectral analysis is the 2D-FDM (filter diagonalization method) (see, e.g., [22]). Even though satisfactory results have been reported using the 2D-FDM, the said method is not fully parametric in the manner of the approach considered in this paper (see below). The list of modes estimated using the 2D-FDM does not separate the signal components from the noise components. The technique suggested herein allows for computation of only the signal parameters corresponding to a (pre-specified) number of signal components.

Consider the following model commonly used for 2D MR data (see, e.g., [7,10])

$$y(t_1,t_2)=\sum_{p=1}^{m}\rho_p\lambda_p^{t_1}\gamma_p^{t_2}+\epsilon(t_1,t_2),$$
$$t_1=0,\ldots,N_1-1,\quad t_2=0,\ldots,N_2-1,$$
$$\lambda_p=\mathrm{e}^{-\alpha_{1p}+\mathrm{i}\omega_{1p}},\quad \gamma_p=\mathrm{e}^{-\alpha_{2p}+\mathrm{i}\omega_{2p}}, \tag{1}$$

where $m$ denotes the total number of signal components, $(\rho_p, \alpha_{qp}, \omega_{qp}; q=1,2)$ are the complex amplitude, dampings and angular frequencies (or simply frequencies, for short) of the $p$th component (note that the sampling period has been absorbed in $\alpha_{qp}$ and $\omega_{qp}$, for notational convenience), $\epsilon(t_1,t_2)$ is a noise term and $N_1$, respectively, $N_2$ denotes the number of available samples in each of the two dimensions (i.e., the collected 2D MRS data can be interpreted as a matrix containing $N_2$ frames, each of length $N_1$). Note that the model in (1) assumes a Lorentzian lineshape for each of the signal components in $\{y(t_1,t_2)\}$. The case of non-Lorentzian lineshapes is beyond the scope of this paper.

Assume that we are interested in estimating only a limited number of the signal components in (1) that are contained in a small region of the 2D spectrum. The number of these components is denoted by

$$n\leqslant m \tag{2}$$

and is assumed to be given. By focusing only on a small region in the spectrum the required computational complexity for estimating the corresponding signal parameters can be decreased significantly. In practice, if we are interested in estimating the signal parameters of all $m$ components this can be done by splitting the total spectral area into several smaller sub-areas where the components are known to lie, and applying the algorithm of this paper to each sub-area.

The considered area comprising the $n$ signal components of interest can be specified by a number of Fourier frequencies in each dimension. In the following we will refer to the spectral dimension corresponding to the modes $\{\lambda_p\}_{p=1}^m$ as the "$k$-dimension" and to the spectral dimension corresponding to the modes $\{\gamma_p\}_{p=1}^m$ as the "$l$-dimension". The two vectors of Fourier frequencies specifying the sub-area of interest are then defined as:

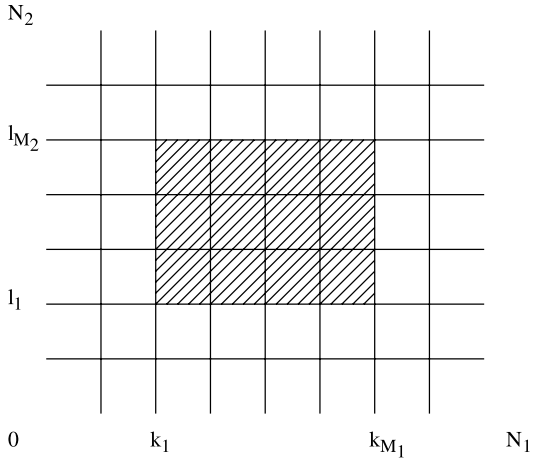


Fig. 1. Graphical illustration showing how to set the parameters $k_1, k_{M_1}, l_1, l_{M_2}$ for a specific area of interest (shaded).

$$k\text{-dimension};\quad \left\{\frac{2\pi k_1}{N_1},\frac{2\pi k_2}{N_1},\ldots,\frac{2\pi k_{M_1}}{N_1}\right\}, \tag{3}$$

$$l\text{-dimension};\quad \left\{\frac{2\pi l_1}{N_2},\frac{2\pi l_2}{N_2},\ldots,\frac{2\pi l_{M_2}}{N_2}\right\}, \tag{4}$$

where $k_1,\ldots,k_{M_1}$, respectively $l_1,\ldots,l_{M_2}$ are integers. A simple illustration showing how to set the parameters $k_1, k_{M_1}, l_1, l_{M_2}$ for a specific area of interest is given in Fig. 1.

2D MRS has been recently used in clinical applications, such as 2D-COSY and 2D-JPRESS (see, e.g., [23,24] and the references therein), and the interest in it is growing. The technique presented in this paper can be used for quantitation of specific signal components in any 2D data experiment. Therefore, the suggested method is outlined in a general manner without referring to the specific notation commonly used in a certain application. Similarly, the presented numerical study is not focused on only one type of MR data nor on a certain clinical application.

In Section 2, we derive a scheme that provides a solution to the area-selective spectral analysis problem introduced above, which we call 2D-ASEEM (area-selective estimation method). The goal is to obtain estimates of the signal parameters $(\rho_p, \alpha_{qp}, \omega_{qp}; q=1,2)$ corresponding to the $n$ signal components located inside the area specified by (3) and (4). In Section 3, we present several numerical examples considering both simulated data and in vitro $^1$H data acquired from a 1.5 T MR scanner. Finally, in Section 4, we provide some concluding remarks.

## 2. 2D-ASEEM

We will start by decomposing the 2D signal processing problem of interest into two 1D estimation problems.

The following derivation, which is inspired by [25] and [26], consists of three main steps:

- Estimation of the modes $\{\lambda_p\}_{p=1}^n$ in the $k$-dimension.
- Estimation of the modes $\{\gamma_p\}_{p=1}^n$ in the $l$-dimension.
- Combined estimation of the complex amplitudes $\{\rho_p\}_{p=1}^n$ and pairing of the estimates of $\{\lambda_p\}_{p=1}^n$ and $\{\gamma_p\}_{p=1}^n$.

We will address these three steps in a one-by-one manner below.

**Step 1.** For estimation of $\{\lambda_p\}_{p=1}^n$ we will use the following notation:

$$w_k = e^{i\frac{2\pi}{N_1}k}, \quad k = 0, \ldots, N_1 - 1, \tag{5}$$

$$\mathbf{u}_k = [w_k \cdots w_k^{S_1}]^T, \tag{6}$$

$$\mathbf{v}_k = [1\, w_k \cdots w_k^{N_1-1}]^T, \tag{7}$$

$$\mathbf{y}_{t_2} = [y(0,t_2) \cdots y(N_1-1,t_2)]^T, \quad t_2 = 0, \ldots, N_2 - 1, \tag{8}$$

$$Y_{kt_2} = \mathbf{v}_k^* \mathbf{y}_{t_2}, \quad k = 0, \ldots, N_1 - 1, \quad t_2 = 0, \ldots, N_2 - 1, \tag{9}$$

where $S_1$ is a user parameter hereafter chosen as $S_1 = \lfloor \frac{M_1}{3} \rfloor$ ($\lfloor \cdot \rfloor$ indicates the integer part) and where $*$ denotes the conjugate transpose. The choice of the user parameter $S_1$ is not critical for the performance of the suggested method (see below for more information on this aspect). The vector $\mathbf{v}_k$ corresponds to the $k$th Fourier vector and hence $\{Y_{kt_2}\}_{k=0}^{N_1-1}$ is the FFT sequence of the $t_2$th data vector $\mathbf{y}_{t_2}$ ($t_2 = 0, \ldots, N_2 - 1$).

For the area-selective analysis in the $k$-dimension we also need the following notation:

$$\mathbf{Y}_{t_2} = [\mathbf{u}_{k_1} Y_{k_1 t_2} \cdots \mathbf{u}_{k_{M_1}} Y_{k_{M_1} t_2}], \tag{10}$$

$$\mathbf{U} = [\mathbf{u}_{k_1} \cdots \mathbf{u}_{k_{M_1}}]. \tag{11}$$

In [26] the following key equation is shown to hold for the 1D scenario (i.e. for a certain value of $t_2$ in our 2D case)

$$\mathbf{Y}_{t_2} = \mathbf{A}\mathbf{X}_{t_2} + \tilde{\mathbf{A}}\tilde{\mathbf{X}}_{t_2} + \mathbf{\Gamma}\mathbf{U} + \boldsymbol{\varepsilon}_{t_2} \tag{12}$$

where the $S_1 \times M_1$ noise matrix $\boldsymbol{\varepsilon}_{t_2}$ is defined similarly to $\boldsymbol{Y}_{t_2}$ for $t_2 = 0, \ldots, N_2 - 1$; also

$$\mathbf{A} = [\mathbf{a}(\lambda_1) \cdots \mathbf{a}(\lambda_n)], \tag{13}$$

$$\mathbf{a}(\lambda_k) = [\lambda_k \cdots \lambda_k^{S_1}]^T, \tag{14}$$

$$\mathbf{X}_{t_2} = [\mathbf{x}_{k_1 t_2} \cdots \mathbf{x}_{k_{M_1} t_2}], \tag{15}$$

$$\mathbf{x}_{kt_2} = \begin{bmatrix} \rho_1 \gamma_1^{t_2} \mathbf{v}_k^* \mathbf{b}(\lambda_1) \\ \vdots \\ \rho_n \gamma_n^{t_2} \mathbf{v}_k^* \mathbf{b}(\lambda_n) \end{bmatrix}, \tag{16}$$

$$\mathbf{b}(\lambda_k) = [1 \;\; \lambda_k \cdots \lambda_k^{N_1-1}]^T \tag{17}$$

for the modes of interest whose frequencies belong to the interval in (3), and similarly $\tilde{\mathbf{A}}$ and $\tilde{\mathbf{X}}_{t_2}$ for the modes outside (3). Note that the matrix $\mathbf{A}$ spans the signal subspace in the $k$-dimension. The matrix $\mathbf{\Gamma}\mathbf{U}$ in (12) can be seen as a remainder term and its explicit expression is of minor importance in this derivation (see below).

Next we assume that

$$M_1 \geqslant n + S_1. \tag{18}$$

Note that we can always choose the user parameter $S_1$ so that the condition in (18) is fulfilled. Besides (18), $S_1$ should also satisfy the inequality $S_1 < \frac{M_1}{2}$ (see, e.g., [2] for more information). In this paper we set $S_1 = \lfloor \frac{M_1}{3} \rfloor$ based on empirical experience. Under (18), the orthogonal projection matrix onto the null space of $\mathbf{U}$ is given by

$$\mathbf{\Pi}_U^{\perp} = \mathbf{I} - \mathbf{U}^*(\mathbf{U}\mathbf{U}^*)^{-1}\mathbf{U}, \tag{19}$$

where $\mathbf{I}$ is the identity matrix. We will eliminate the third term in (12) by post-multiplying this equation with $\mathbf{\Pi}_U^{\perp}$ (see below). However, before doing so we briefly discuss the contribution from the second and fourth terms in (12). The elements of the noise term $\boldsymbol{\varepsilon}_{t_2}$ are usually much smaller than the elements of $\mathbf{A}\mathbf{X}_{t_2}$. In addition, assuming that the out-of-area components are not much stronger than the components in the area of interest and that the frequencies of the former are not too close to the interval in (3), the elements of $\tilde{\mathbf{X}}_{t_2}$ are also much smaller than the elements of $\mathbf{X}_{t_2}$. Following the discussion in [26], it can be argued that even if the frequency of an interfering signal component is relatively close to the area of interest, we can expect that the "spectral tail" of the out-of-area component may well have a small dynamic range in the area of interest. In addition, it is shown in [26] that both the second and fourth term in (12) are roughly proportional to $\mathbf{U}$. As a consequence, the out-of-area components and the noise term in (12) will be attenuated via the post-multiplication by $\mathbf{\Pi}_U^{\perp}$.

It follows from the previous discussion that

$$\mathbf{Y}_{t_2}\mathbf{\Pi}_U^{\perp} \approx \mathbf{A}\mathbf{X}_{t_2}\mathbf{\Pi}_U^{\perp}, \quad t_2 = 0, \ldots, N_2 - 1. \tag{20}$$

Due to the exponential damping in the $l$-dimension, the signal-to-noise ratio (SNR) in (20) drops quickly as $t_2$ increases. In the numerical example section we will use (20) only for $t_2 = 0, \ldots, \lfloor \frac{N_2}{50} \rfloor + 1$ (assuming $N_2 \geqslant 256$) for estimation of the modes $\{\lambda_p\}_{p=1}^n$, to avoid including low-SNR frames. Our empirical experience is that the estimation performance does not change significantly when the number of considered frames is taken as any small fraction of the total number of available frames. We construct a matrix $\mathbf{Y}$ given by

$$\mathbf{Y} = \sum_{t_2=1}^{\lfloor \frac{N_2}{50} \rfloor + 1} \mathbf{Y}_{t_2}\mathbf{\Pi}_U^{\perp} \approx \mathbf{A}\left( \sum_{t_2=1}^{\lfloor \frac{N_2}{50} \rfloor + 1} \mathbf{X}_{t_2} \right)\mathbf{\Pi}_U^{\perp}. \tag{21}$$

Note that the effective rank of $\mathbf{Y}$ is equal to $n$. Thus, we can use a standard SVD-based technique (see, e.g., [2] and below) to retrieve the modes $\{\lambda_p\}_{p=1}^n$ from $\mathbf{Y}$.

Let $\mathbf{W}$ be the $S_1 \times n$ matrix whose columns are the left singular vectors of $\mathbf{Y}$ associated with the $n$ largest singular values. In addition, let

$$\mathbf{W}_u = [\mathbf{I}_{S_1-1} \; 0]\mathbf{W}, \tag{22}$$

$$\mathbf{W}_d = [0 \; \mathbf{I}_{S_1-1}]\mathbf{W}, \tag{23}$$

and let

$$\mathbf{\Phi} = (\mathbf{W}_u^* \mathbf{W}_u)^{-1} \mathbf{W}_u^* \mathbf{W}_d. \tag{24}$$

Estimates of the modes $\{\lambda_p\}_{p=1}^n$ can be obtained as the eigenvalues of $\mathbf{\Phi}$ (see, e.g., [2]).

**Step 2.** Estimates of the modes $\{\gamma_p\}_{p=1}^n$ are obtained transposing the collected data matrix in (1) and applying to it a frequency-selective scheme, similar to Step 1, in the $l$-dimension.

**Step 3.** Finally, we need to pair the estimates of $\{\lambda_p\}_{p=1}^n$ and $\{\gamma_p\}_{p=1}^n$ to obtain a correct set of estimated signal modes $\{\hat{\lambda}_p, \hat{\gamma}_p\}_{p=1}^n$. We also need to compute estimates $\{\hat{\rho}_p\}_{p=1}^n$ of the complex amplitudes $\{\rho_p\}_{p=1}^n$. Both operations can be performed simultaneously by minimizing the sum of squared errors between the original data and the reconstructed noise-free data, in the frequency domain, with respect to $\{\rho_p\}_{p=1}^n$. This minimization has to be performed for all possible pairs $\{\hat{\lambda}_p, \hat{\gamma}_p\}_{p=1}^n$. Since the number of signal components inside the area of interest is usually low, we do not need to test more than a few combinations. By letting $\mathbf{Y}^F$ denote the 2D-FFT of $\{y(t_1, t_2)\}$

$$\mathbf{Y}^F(k,l) = \sum_{t_1=0}^{N_1-1} \sum_{t_2=0}^{N_2-1} y(t_1,t_2) \mathrm{e}^{-\mathrm{i}\frac{2\pi}{N_1}k} \mathrm{e}^{-\mathrm{i}\frac{2\pi}{N_2}l},$$
$$k = k_1, \ldots, k_{M_1}, \quad l = l_1, \ldots, l_{M_2} \tag{25}$$

the minimization problem can be written as

$$\min_{\{\rho_p\}} \sum_{k=k_1}^{k_{M_1}} \sum_{l=l_1}^{l_{M_2}} |\mathbf{Y}^F(k,l) - \sum_{p=1}^{n} \rho_p \mathbf{C}_p(k,l)|^2 \tag{26}$$

where $\mathbf{C}_p$ is defined as the 2D-FFT of the reconstructed data for the $p$th component based on a specific pairing combination $\{\hat{\lambda}_p, \hat{\gamma}_p\}_{p=1}^n$

$$\mathbf{C}_p(k,l) = \sum_{t_1=0}^{N_1-1} \sum_{t_2=0}^{N_2-1} \hat{\lambda}_p^{t_1} \hat{\gamma}_p^{t_2} \mathrm{e}^{-\mathrm{i}\frac{2\pi}{N_1}k} \mathrm{e}^{-\mathrm{i}\frac{2\pi}{N_2}l},$$
$$k = k_1, \ldots, k_{M_1}, \quad l = l_1, \ldots, l_{M_2}. \tag{27}$$

The solution to (26) can be obtained as

$$\hat{\boldsymbol{\rho}} = \begin{bmatrix} \hat{\rho}_1 \\ \vdots \\ \hat{\rho}_n \end{bmatrix} = \left( \sum_{l=l_1}^{l_{M_2}} \begin{bmatrix} \mathbf{c}_1^*(l) \\ \vdots \\ \mathbf{c}_n^*(l) \end{bmatrix} [\mathbf{c}_1(l) \ \cdots \ \mathbf{c}_n(l)] \right)^{-1} \times \left( \sum_{l=l_1}^{l_{M_2}} \begin{bmatrix} \mathbf{c}_1^*(l)\mathbf{y}^F(l) \\ \vdots \\ \mathbf{c}_n^*(l)\mathbf{y}^F(l) \end{bmatrix} \right), \tag{28}$$

where $\mathbf{c}_p(l)$ and $\mathbf{y}^F(l)$ are the $l$th columns of the matrices $\mathbf{C}_p$ and $\mathbf{Y}^F$ whose elements are $\{\mathbf{C}_p(k,l)\}$ and $\{\mathbf{Y}^F(k,l)\}$. The pairing procedure is completed by selecting the combination $\{\hat{\lambda}_p, \hat{\gamma}_p\}_{p=1}^n$ which gives the smallest sum of squared errors in (26).

**Remark.** The case of non-distinct frequencies in either dimension has been studied often in the previous literature on 2D spectral analysis. Using the approach outlined above, this problem can be taken care of easily. For the case of non-distinct frequencies in the considered dimension the true number of frequencies is lower than the number of estimated frequencies ($n$), and hence we obtain spurious frequency estimates. It is most likely that such spurious frequency estimates are located well outside the sub-area of interest, and therefore they can be easily disregarded. If a spurious frequency estimate happens to lie within the selected sub-area it has to be included in (26). However, since we select only the pair $\{\hat{\lambda}_p, \hat{\gamma}_p\}_{p=1}^n$ which gives the minimum value of (26), spurious frequency pairs are likely to be eliminated.

## 3. Numerical examples

We consider five different numerical examples below to illustrate the performance of the suggested technique, namely:

- A simulated 2 component data example where we estimate the signal parameters of one small component located in the spectral tail of a large nuisance component.
- A simulated 11 component data example where we estimate the signal parameters of two rather closely spaced components.
- A modified case of the 11 component data example above where the two components have identical frequencies in the $k$-dimension.
- A simulated 5 component data example mimicking the experimental data example in [10].
- An in vitro data example based on phantom $^1$H data.

### 3.1. Simulated 2 component data

Consider a 2 component 2D signal as in (1). The added noise is zero mean, white and Gaussian distributed with standard deviation $\sigma$. Below the statistical parameter estimation performance of 2D-ASEEM is presented for different levels of noise. For comparison we also include the temporal Cramér-Rao Bounds (CRBs) as lower bounds on the variances of the signal parameter estimates (see, e.g., [2]). Note that the CRBs are strictly valid only for an unbiased estimator (see [27]), which is not necessarily the case here. However, the CRBs are still useful for a qualitative performance analysis. The quality of the different parameter estimates is measured as the relative root mean square error (RRMSE) for each component $p = 1, \ldots, n$ [in percent]:

$$\mathrm{RRMSE}_p \triangleq 100 \sqrt{\frac{1}{\Upsilon} \sum_{\upsilon=1}^{\Upsilon} \frac{(\xi_p - \hat{\xi}_p^{\upsilon})^2}{\xi_p^2}}, \tag{29}$$

where $\Upsilon$ is the number of Monte-Carlo (MC) runs (we use 1000 here), $\xi_p$ denotes the relevant parameter and $\hat{\xi}_p^{\upsilon}$ is its estimate obtained in the $\upsilon$th run.

The parameters of the 2 signal components are presented in Table 1. The number of samples of the considered data matrix is $1024 \times 256$ (i.e., the length of each FID is $N_1 = 1024$ and we consider $N_2 = 256$ collected frames). The sampling frequency is 1 kHz. We focused on the small component (component 1 in Table 1) to illustrate the estimation performance of 2D-ASEEM when the component of interest is affected by the spectral tail of a strong nuisance component (component 2 in Table 1) lying outside the selected spectral area. This is a common scenario for example in $^1$H MRS when the (residual) water component is much stronger than the signal component(s) of interest. The considered spectral area is relatively small compared to the full spectral range. The lower frequency bounds $k_1$ and $l_1$ were set to 15 Hz, respectively, 8 Hz and the higher frequency bounds $k_{M_1}$ and $l_{M_2}$ were set to 25, respectively 31 Hz, which corresponds to $M_1 = 11$ and $M_2 = 7$. The RRMSEs for the parameters of interest (frequencies, dampings, and amplitudes) are shown in Figs. 2–4 for component 1 for increasing noise standard deviation.

From Figs. 2–4, we see that the statistical parameter estimation performance of the suggested method is comparable to the CRBs for this example. In Figs. 2 and 3 the RRMSEs for $\omega_{21}$ and $\alpha_{21}$ obtained using 2D-ASEEM are sometimes lower than the corresponding CRBs. This phenomenon can occur in a practical scenario due to the use of a biased estimation method [27]. Note that $\sigma = 50$ corresponds to a very low SNR since the amplitude of the considered signal component is equal to 20 (see Table 1). The reason why we let $\sigma$ take on such large values is to show that even in the low SNR case the parameter estimates obtained using the suggested technique are relatively close to the CRBs.

Table 1
Signal parameters in the 2 component simulated data case; $\omega_{qp}, q = 1,2$ are the frequencies, $\alpha_{qp}, q = 1,2$ are the dampings, $|\rho_p|$ denote the amplitudes, and $\arg(\rho_p)$ are the phases (where $\arg(\cdot)$ denotes the argument)

| $p$ | $\omega_{1p}$ (Hz) | $\omega_{2p}$ (Hz) | $\alpha_{1p}$ | $\alpha_{2p}$ | $\rho_p$ |
|---|---|---|---|---|---|
| 1 | 20 | 20 | 0.01 | 0.01 | 20 ($e^{i\pi/2}$) |
| 2 | 100 | 100 | 0.01 | 0.01 | 320 ($e^{i\pi/2}$) |

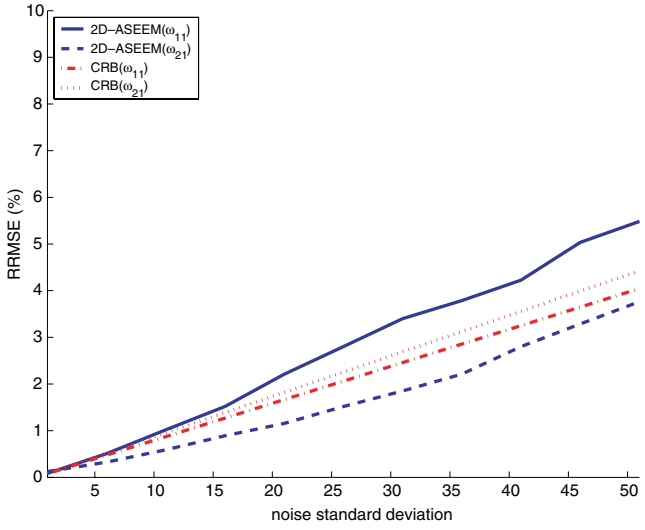


Fig. 2. Frequency RRMSEs for component 1 in the simulated 2 component data example using 1000 MC runs.

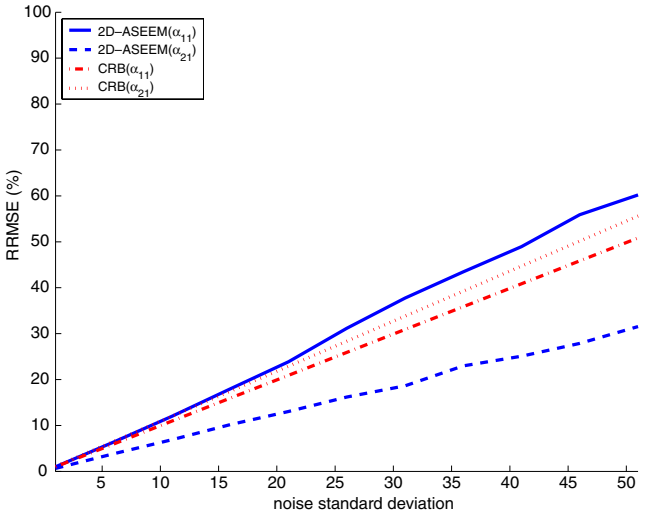


Fig. 3. Damping RRMSEs for component 1 in the simulated 2 component data example using 1000 MC runs.

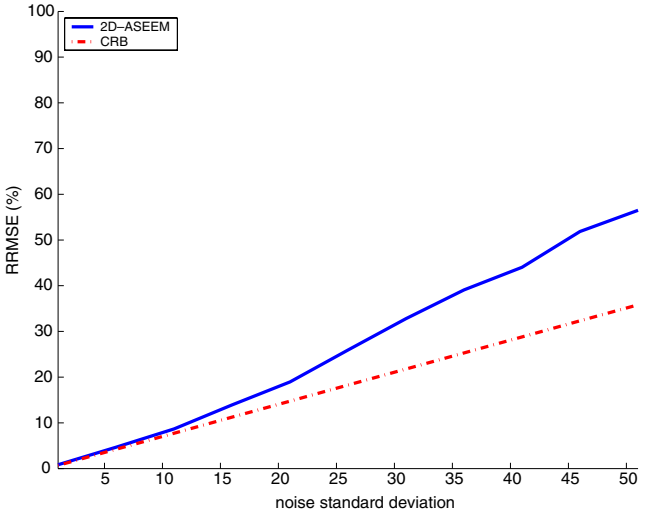


Fig. 4. Amplitude RRMSEs for component 1 in the simulated 2 component data example using 1000 MC runs.

For comparison purposes we also show the (zero-padded) 2D-FFT spectra, for the area of interest, of both the original data and of the reconstructed data obtained using the signal parameters estimated by 2D-ASEEM. The presented results are for a typical run using a noise standard deviation equal to 30. All other user parameters are selected as above. The resulting spectra are shown in Fig. 5 and the signal parameter estimates obtained using 2D-ASEEM are shown in Table 2. At this relatively low SNR the standard 2D-FFT fails to provide a distinct and reliable spectral estimate of component 1. However, the estimates

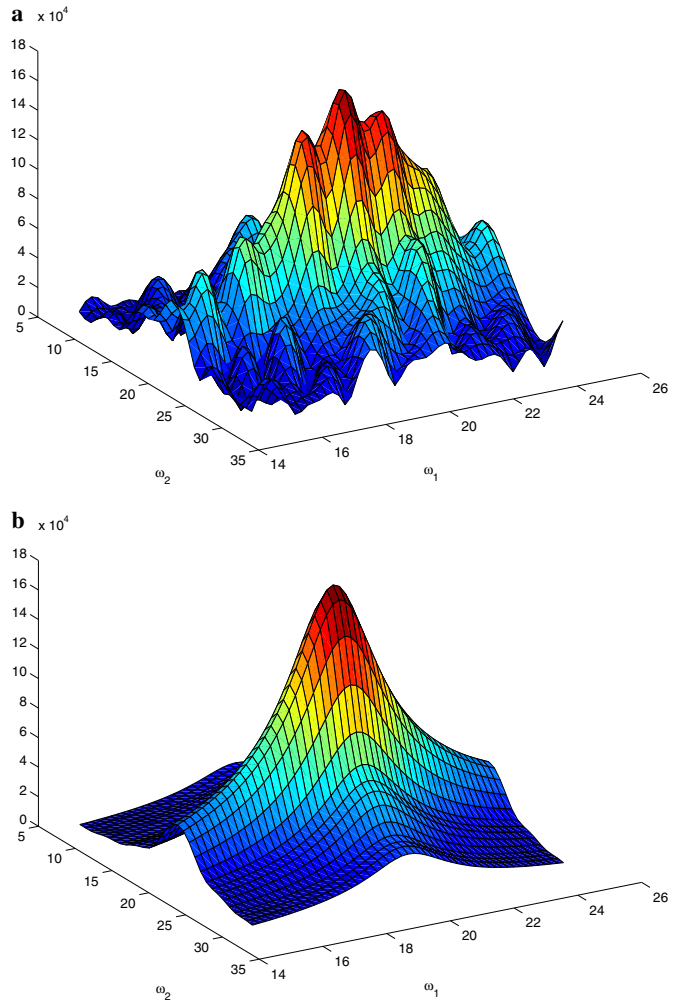


Fig. 5. 2D-FFT spectra of both the original data (a) and of the reconstructed data obtained using the signal parameters estimated by 2D-ASEEM (b) in the simulated 2 component data case.

Table 2
Parameter estimates of component 1 obtained for one typical run using 2D-ASEEM in the simulated 2 component data case when $\sigma = 30$

| $p$ | $\omega_{1p}$ (Hz) | $\omega_{2p}$ (Hz) | $\alpha_{1p}$ | $\alpha_{2p}$ | $\rho_p$ |
|---|---|---|---|---|---|
| 1 | 19.48 | 19.81 | 0.0087 | 0.0104 | 17.97 ($e^{i\pi 1.18/2}$) |

obtained using 2D-ASEEM are close to the true parameter values. In addition, the reconstructed spectrum based on the 2D-ASEEM signal parameter estimates contains little noise or artifacts from out-of-area components.

### 3.2. Simulated 11 component data

In this subsection we consider a simulated 11 component 2D data example. As in the previous 2 component example the added noise is zero mean, white and Gaussian distributed with standard deviation $\sigma$. The parameters of the 11 signal components are presented in Table 3. The number of samples of the considered data matrix is $512 \times 512$. The sampling frequency is 3 kHz. We focused on estimating the parameters of components 4 and 5 in Table 3. The considered spectral area is again relatively small compared to the full spectral range. The lower frequency bounds $k_1$ and $l_1$ were set to 129 Hz and the higher frequency bounds $k_{M_1}$ and $l_{M_2}$ were set to 193 Hz, which corresponds to $M_1 = M_2 = 12$. The RRMSEs for the frequencies, dampings, and amplitudes for components 4 and 5 are shown in Figs. 6–8 for increasing noise standard deviation. As in the previous example (Section 3.1) we note that the increase of the RRMSE in Figs. 6–8 is approximately linear in the noise standard deviation which indicates a robust performance. Moreover, the RRMSEs are well under 50% for all values of the noise standard deviation used in this example.

### 3.3. Simulated 11 component data with non-distinct frequencies

In order to show the performance of the suggested technique in the case where two signal components have identical frequencies in the $k$-dimension we modify the previous 11 component signal example slightly. The modifications refer to components 4 and 5 and are shown in Table 4.

Table 3
Signal parameters in the 11 component simulated data case; $\omega_{qp}, q = 1,2$ are the frequencies, $\alpha_{qp}, q = 1,2$ are the dampings, $|\rho_p|$ denote the amplitudes, and $\arg(\rho_p)$ are the phases

| $p$ | $\omega_{1p}$ (Hz) | $\omega_{2p}$ (Hz) | $\alpha_{1p}$ | $\alpha_{2p}$ | $\rho_p$ |
|---|---|---|---|---|---|
| 1 | −86 | −86 | 0.0167 | 0.0167 | 75 ($e^{i0.75\pi}$) |
| 2 | −70 | −70 | 0.0167 | 0.0167 | 150 ($e^{i0.75\pi}$) |
| 3 | −54 | −54 | 0.0167 | 0.0167 | 75 ($e^{i0.75\pi}$) |
| 4 | 152 | 152 | 0.0167 | 0.0167 | 150 ($e^{i0.75\pi}$) |
| 5 | 168 | 168 | 0.0167 | 0.0167 | 150 ($e^{i0.75\pi}$) |
| 6 | 292 | 292 | 0.0167 | 0.0167 | 150 ($e^{i0.75\pi}$) |
| 7 | 308 | 308 | 0.0167 | 0.0167 | 150 ($e^{i0.75\pi}$) |
| 8 | 360 | 360 | 0.0083 | 0.0083 | 150 ($e^{i0.75\pi}$) |
| 9 | 440 | 440 | 0.0951 | 0.0951 | 1400 ($e^{i0.75\pi}$) |
| 10 | 490 | 490 | 0.0083 | 0.0083 | 60 ($e^{i0.75\pi}$) |
| 11 | 530 | 530 | 0.0666 | 0.0666 | 500 ($e^{i0.75\pi}$) |

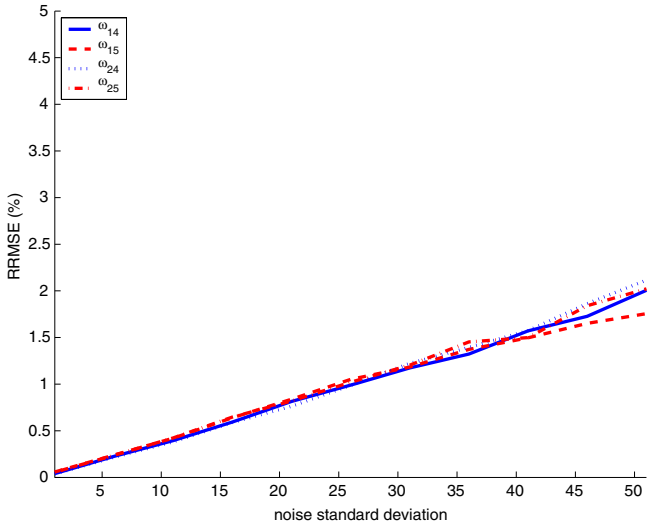


Fig. 6. Frequency RRMSEs for components 4 and 5 in the simulated 11 component data example using 1000 MC runs.

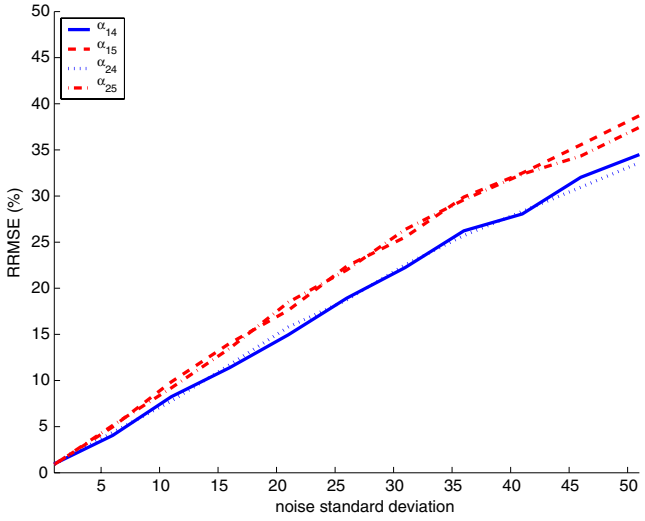


Fig. 7. Damping RRMSEs for components 4 and 5 in the simulated 11 component data example using 1000 MC runs.

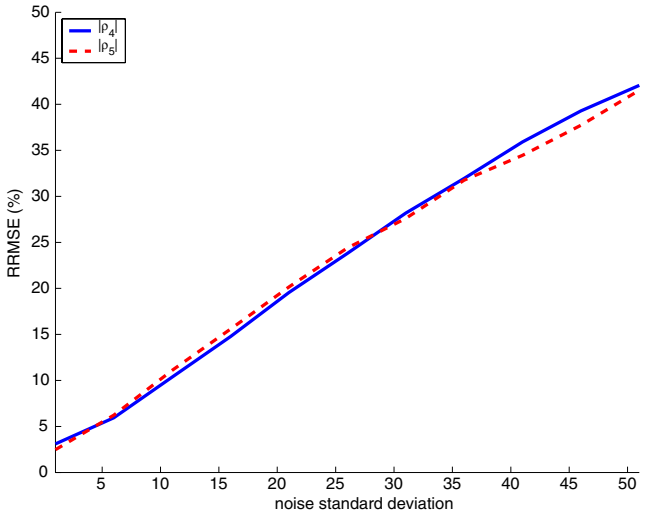


Fig. 8. Amplitude RRMSEs for components 4 and 5 in the simulated 11 component data example using 1000 MC runs.

All other data parameters are kept as in the 11 component example in Section 3.2. The RRMSEs for the frequencies, dampings, and amplitudes for components 4 and 5 are shown in Figs. 9–11 for increasing noise standard deviation. The numerical results in Figs. 9–11 are similar to those in the previous example (Section 3.2). The main difference is that the RRMSEs of $\omega_{1p}$ and $\alpha_{1p}$ $(p = 1,2)$ in Figs. 9 and 10 are lower than those in Figs. 6, 7. This is probably due to the fact that we implicitly use the information that $\omega_{14} = \omega_{15}$ when estimating the parameters (i.e., we estimate the same parameters $\omega_{1p}$ and $\alpha_{1p}$ $(p = 1,2)$ for two different components).

### 3.4. Simulated 5 component data mimicking experimental data

In this section, we consider simulated data mimicking the experimental data example used in [10]. The original data set in [10] was obtained from the National Institute of Health (NIH). Because we do not have access to the experimental data, we will use the estimated signal parameters given in [10] as the true values of the signal parameters to be estimated by 2D-ASEEM (see Table 5). In addition, we move one of the components so that there are two closely spaced components ($p = 2,3$ in Table 5) which the conventional 2D-FFT cannot resolve. The

Table 4
Parameters of the modified components 4 and 5 in the simulated data case where $\omega_{14} = \omega_{15}$

| $p$ | $\omega_{1p}$ (Hz) | $\omega_{2p}$ (Hz) | $\alpha_{1p}$ | $\alpha_{2p}$ | $\rho_p$ |
|---|---|---|---|---|---|
| 4 | 160 | 152 | 0.0167 | 0.0167 | 150 ($e^{i0.75\pi}$) |
| 5 | 160 | 168 | 0.0167 | 0.0167 | 150 ($e^{i0.75\pi}$) |

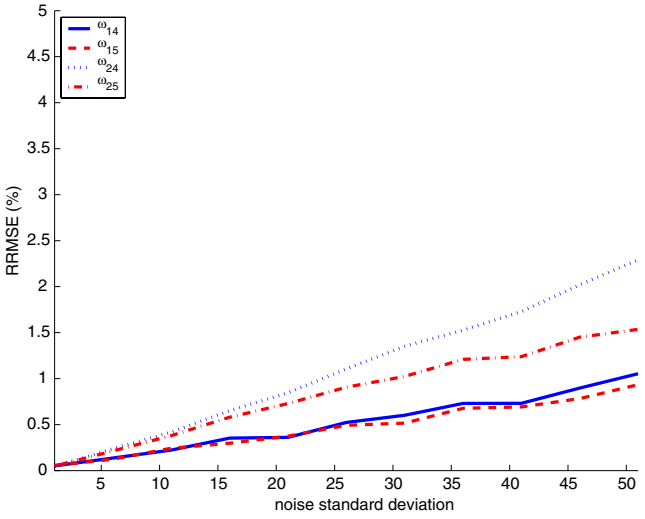


Fig. 9. Frequency RRMSEs for the modified components 4 and 5 in the simulated data example where $\omega_{14} = \omega_{15}$ using 1000 MC runs.

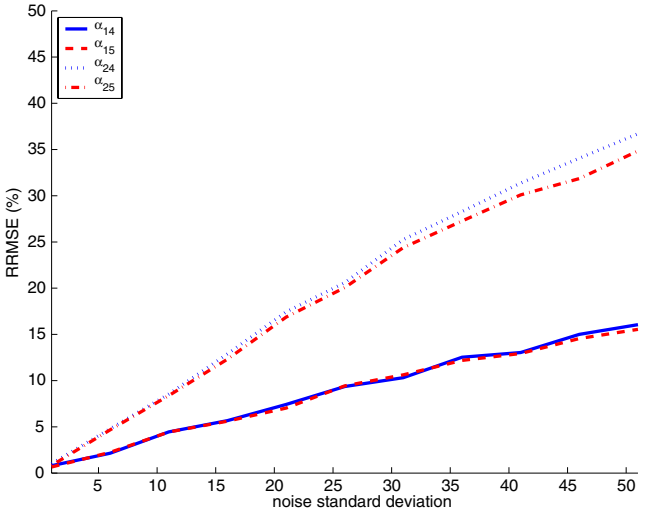


Fig. 10. Damping RRMSEs for the modified components 4 and 5 in the simulated data example where $\omega_{14} = \omega_{15}$ using 1000 MC runs.

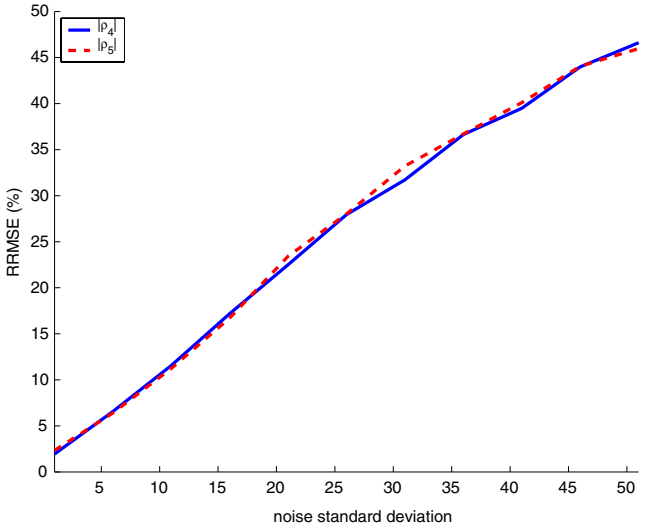


Fig. 11. Amplitude RRMSEs for the modified components 4 and 5 in the simulated data example where $\omega_{14} = \omega_{15}$ using 1000 MC runs.

Table 5
Signal parameters in the 5 component simulated data case; $\omega_{qp}, q = 1,2$ are the frequencies, $\alpha_{qp}, q = 1,2$ are the dampings, $|\rho_p|$ denote the amplitudes, and $\arg(\rho_p)$ are the phases

| $p$ | $\omega_{1p}$ (Hz) | $\omega_{2p}$ (Hz) | $\alpha_{1p}$ | $\alpha_{2p}$ | $\rho_p$ |
|---|---|---|---|---|---|
| 1 | 0.200 | −0.010 | 0.06 | 0.06 | 70 ($e^{i0.50\pi}$) |
| 2 | −0.225 | 0.185 | 0.07 | 0.08 | 100 ($e^{i0.50\pi}$) |
| 3 | −0.210 | 0.200 | 0.07 | 0.09 | 100 ($e^{i0.50\pi}$) |
| 4 | 0.050 | −0.060 | 0.13 | 0.09 | 120 ($e^{i0.50\pi}$) |
| 5 | 0.060 | 0.320 | 0.21 | 0.29 | 400 ($e^{i0.50\pi}$) |

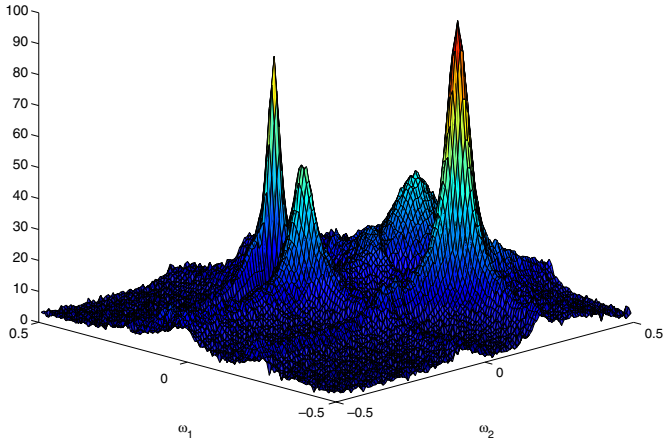


Fig. 12. 2D-FFT spectrum of the simulated 5 component data mimicking the experimental NIH data in [10].

number of samples of the considered data matrix is $120 \times 120$. In Fig. 12 we show the 2D-FFT spectrum obtained for one typical noise realization. The signal contains 5 components and the SNR is approximately 30 dB. In Fig. 13, we present a contour plot where the selected sub-area is represented as a small square centered on component 2 and 3 in Table 5. The size of the selected sub-area

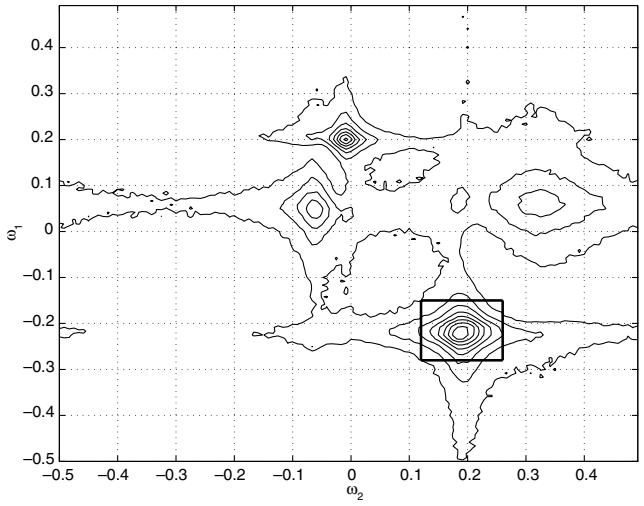


Fig. 13. Contour plot of the simulated 5 component data mimicking the experimental NIH data in [10] where the selected sub-area is marked as a small square.

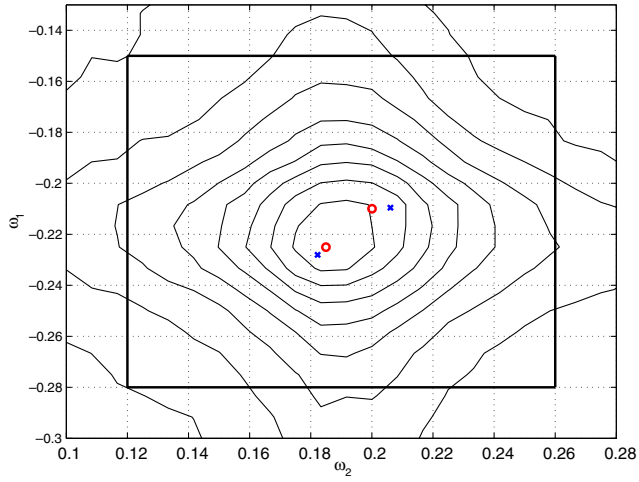


Fig. 14. Zoom of the sub-area of interest in Fig. 13 where the true frequencies are indicated with small circles and their estimates obtained using 2D-ASEEM are indicated with small x-marks.

is $M_1 = M_2 = 13$. In Fig. 14 we also show a zoom of the sub-area of interest in Fig. 13 together with the true frequencies indicated with small circles and their estimates obtained using 2D-ASEEM indicated with small x-marks. We note that the frequency estimates obtained using the suggested technique are very close to the true values.

### 3.5. In vitro data

The suggested approach was tested on experimental 2D MR spectroscopic data. We consider a GE MRS phantom with known solutions of metabolites with the following concentrations: 12.5 mM NAA, 10.0 mM creatine (Cr), 3.0 mM choline (Ch), 7.5 mM myoinositol (mI), 12.5 mM L-glutamic acid (Glu), 5.0 mM lactate, and 0.5 mM γ-aminobutyric acid (GABA). Data were collected on a 1.5 T GE

Signa MR scanner using a single channel quadrature head coil manufactured by GE Healthcare Technologies, Milwaukee, WI, USA. An MR pulse sequence developed for breast spectroscopy (BREASE) was used to acquire the data. The region of interest for this MRS experiment was an 8 $cm^3$ volume located at iso-center. Each frame of data was averaged from 16 acquisitions (NEX = 16). Prior to processing phase-correction and water removal was performed using non-water-suppressed reference data (see [28] for more information). TR was 2000 ms, receiver bandwidth was 2500 Hz, and $N_1 = 2048$ complex valued points were sampled for each of the $N_2 = 64$ readouts. Each frame of data corresponds to a different TE at equally spaced intervals from 25 to 345 ms. Total scan time was 38 min and 40 s.

In Fig. 15 we show, similarly to Fig. 5 in the simulated 2 component data case, the original and the reconstructed 2D-FFT spectra, focusing on the choline component that is of main interest in the BREASE application since it is often associated with cancerous tumors. The size of the selected sub-area was $M_1 = 12$ and $M_2 = 10$. Since the number of frames ($N_2$) is only 64 in this example we use the first 6 frames in (21), instead of the recommended $\lfloor \frac{N_2}{50} \rfloor + 1$, for estimation of $\lambda$.

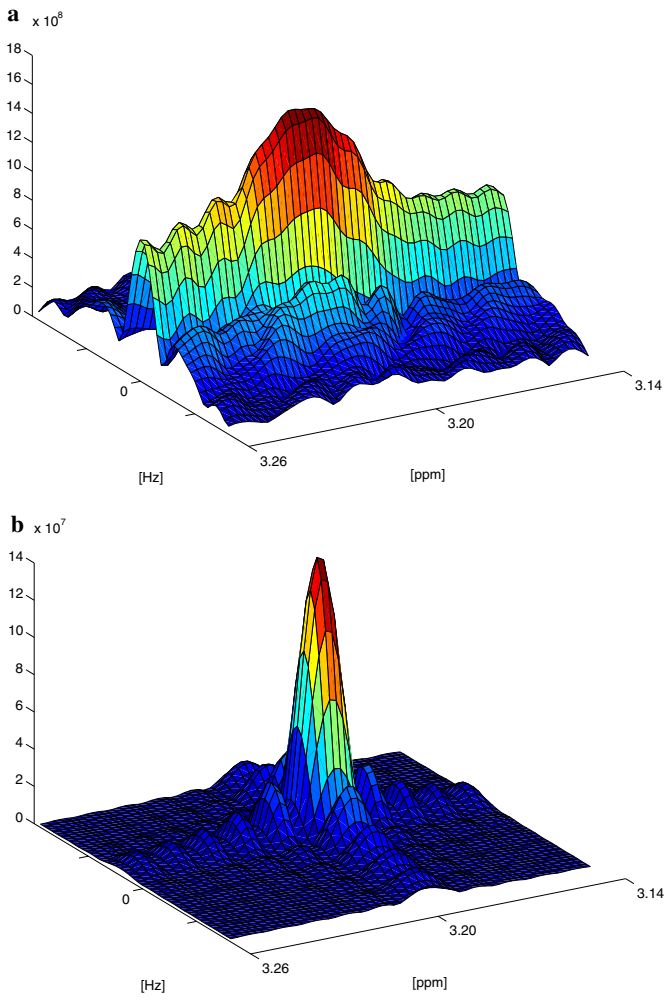


Fig. 15. 2D-FFT spectra of both the original data (a) and of the reconstructed data obtained using the signal parameters estimated by 2D-ASEEM (b) in the in vitro $^1H$ data case.

The signal component in the two spectra have similar frequency estimates. The difference between the original and the reconstructed spectra is again related to the fact that the 2D-ASEEM estimates are not significantly corrupted by the spectral tails of strong adjacent components (such as the water component) that lie outside the selected area, nor by the measurement noise. Hence we can use the suggested 2D-ASEEM method especially in scenarios where the component(s) of interest cannot be easily estimated using the conventional 2D-FFT.

## 4. Conclusions

A computationally efficient area-selective 2D parametric spectral analysis technique was suggested that can be used to estimate the parameters of selected components for large-size data sequences for which parametric estimates are usually difficult to obtain by using a full-band method. The proposed approach can be used in any 2D MRS data application, regardless of the pulse sequence or the specific instrumentation employed. The technique attenuates effectively the interference from measurement noise and out-of-area components, which in the MRS data case can be dominant. The full spectral area can be divided into several smaller sub-areas and the proposed technique can be applied to each sub-area, if estimation of all signal components in the data is of interest. The obtained parameter estimates can also be used to reconstruct a noise-free signal containing only the selected components.

## Acknowledgment

The authors are grateful to David H. Gurr, GE Healthcare Technologies, for his help in collecting the in vitro BREASE data used in the numerical example section.

## References

[1] J. Jeener, Lecture Notes About Two-dimensional NMR Spectroscopy, Ampere International Summer School, Basko polje, Yugoslavia, 1971.
[2] P. Stoica, R. Moses, Spectral Analysis of Signals, Prentice Hall, Upper Saddle River, NJ, 2005.
[3] H. Gesmar, J.J. Led, Spectral estimation of two-dimensional NMR signals applying linear prediction to both dimensions, J. Magn. Reson. 76 (1988) 575–586.
[4] C.F. Tirendi, J.F. Martin, Fast linear prediction processing in two-dimensional NMR spectroscopy, J. Magn. Reson. 81 (1989) 577–585.
[5] Y. Hua, Estimating two-dimensional frequencies by matrix enhancement and matrix pencil, IEEE Trans. Sign. Proc. 40 (1992) 2267–2280.
[6] Y. Hua, F. Baqai, Correction to: "Estimating two-dimensional frequencies by matrix enhancement and matrix pencil", IEEE Trans. Sign. Proc. 42 (1994) 1288.
[7] Y. Zhu, Y. Hua, Spectral estimation of two-dimensional NMR signals by matrix pencil method, Proc. Comp. Commun. Control Power Eng. 3 (1993) 546–549.

[8] S. Rouquette, M. Najim, Estimation of frequencies and damping factors by two-dimensional ESPRIT methods, IEEE Trans. Sign. Proc. 49 (2001) 237–245.
[9] Y. Wang, J.-W. Chen, Z. Liu, Comments on: ''Estimation of frequencies and damping factors by two-dimensional ESPRIT methods'', IEEE Trans. Sign. Proc. 53 (2005) 237–245.
[10] Y. Li, J. Razavilar, K.J. Ray Liu, A high-resolution technique for multidimensional NMR spectroscopy, IEEE Trans. Biomed. Eng. 45 (1998) 78–86.
[11] M. Viberg, P. Stoica, A computationally efficient method for joint direction finding and frequency estimation in colored noise, Proc. Asilomar Sign., Syst. Comp. 2 (1998) 1547–1551.
[12] G.F. Hatke, K.W. Forsythe, A class of rooting algorithms for joint azimuth/elevation estimation using multidimensional arrays, Proc. Asilomar Sign., Syst. Comp. 1 (1994) 694–699.
[13] F. Athley, Asymptotically decoupled angle-frequency estimation with sensor arrays, Proc. Asilomar Sign., Syst. Comp. 2 (1999) 1098–1102.
[14] M.D. Zoltowski, M. Haardt, C.P. Mathews, Closed-form 2-D angle estimation with rectangular arrays in element space or beamspace via unitary ESPRIT, IEEE Trans. Sign. Proc. 44 (1996) 316–328.
[15] L. Vanhamme, T. Sundin, P. Van Hecke, S. Van Huffel, R. Pintelon, Frequency-selective quantification of biomedical magnetic resonance spectroscopy data, J. Magn. Reson. 143 (2000) 1–16.
[16] I. Dologlou, S. Van Huffel, D. van Ormondt, Frequency-selective MRS data quantification with frequency prior knowledge, J. Magn. Reson. 130 (1998) 238–243.
[17] R. Romano, A. Motta, S. Camassa, C. Pagano, M.T. Santini, P.L. Indovina, A new time-domain frequency-selective quantification algorithm, J. Magn. Reson. 155 (2002) 226–235.
[18] S. Cavassila, B. Fenet, A. van den Boogaart, C. Rémy, C. Briguet, D. Graveron-Demilly, ER-filter: a preprocessing technique to improve the performance of SVD-based quantitation methods, J. Magn. Reson. Anal. 3 (1997) 87–92.
[19] J. Tang, J.R. Norris, LP-ZOOM, a linear prediction method for local spectral analysis of NMR signals, J. Magn. Reson. 79 (1988) 190–196.
[20] J. Slotboom, C. Boesch, R. Kreis, Versatile frequency domain fitting using time domain models and prior knowledge, Magn. Reson. Med. 39 (1998) 899–911.
[21] M.R. Wall, D. Neuhauser, Extraction, through filter-diagonalization, of general quantum eigenvalues or classical normal mode frequencies from a small number of residues or a short-time segment of a signal. I. Theory and application to a quantum-dynamics model, J. Chem. Phys. 102 (1995) 8011–8022.
[22] V.A. Mandelshtam, H.S. Taylor, Multidimensional harmonic inversion by filter-diagonalization, J. Chem. Anal. 108 (1998) 9970–9977.
[23] M.A. Thomas, N. Hattori, M. Umeda, T. Sawada, S. Naruse, Evaluation of two-dimensional L-COSY and JPRESS using a 3T MRI scanner: from phantoms to human brain in vivo, NMR Biomed. 16 (2003) 245–251.
[24] E. Adalsteinsson, D.M. Spielman, Spatially resolved two-dimensional spectroscopy, Magn. Reson. Med. 41 (1999) 8–12.
[25] T. McKelvey, M. Viberg, A robust frequency domain subspace algorithm for multi-component harmonic retrieval, in: Proc. of 35th Asilomar Conf. on Signals, Systems and Computers, Nov, 2001, pp. 68–72.
[26] P. Stoica, N. Sandgren, Y. Selén, L. Vanhamme, S. Van Huffel, Frequency-domain method based on the singular value decomposition for frequency-selective NMR spectroscopy, J. Magn. Reson. 165 (2003) 80–88.
[27] P. Stoica, R. Moses, On biased estimators and the unbiased Cramér-Rao lower bound, Sign. Proc. 21 (1990) 349–350.
[28] B.J. Soher, R.E. Hurd, N. Sailasuta, P.B. Barker, Quantitation of automated single-voxel proton MRS using cerebral water as an internal reference, Magn. Reson. Med. 36 (1996) 335–339.